

Missing Physics Discovery through Fully Differentiable Finite Element-Based Machine Learning

Ado Farsi^{*1,2,3}, Nacime Bouziani^{†3,4,5}, and David A. Ham^{‡4}

¹Imperial College London, Earth Science and Engineering Department, London, United Kingdom

²University College London, Earth Sciences Department, London, United Kingdom

³Tanuki Technologies, London, United Kingdom

⁴Imperial College London, Department of Mathematics, London, United Kingdom

⁵Amazon Science UK, London, United Kingdom

ABSTRACT

Modelling complex physical systems through partial differential equations (PDEs) is central to many disciplines in science and engineering. However, in most real applications, missing physics within the PDE model, expressed as unknown or incomplete relationships, such as constitutive or thermal laws, limits the description of the physics of interest. Existing surrogate modelling approaches aim to address this knowledge gap by learning the PDE solution directly from data, and in some cases, by also adding known physical constraints. However, these approaches are tailored and tied to specific system configurations (e.g., geometries, boundary conditions, or discretisations) and do not directly learn the missing physics, but only the PDE solution. We introduce FEML, an end-to-end differentiable framework for learning missing physics that combines the PDE modelling of the system of interest (known physics) with ML modelling of the operator representing the missing physics. By embedding a PDE solver into training, our approach allows one to train such operators directly from the PDE solution, which unlocks the learning of unknown relationships when the operator output cannot be directly measured (e.g., stress signals for learning constitutive models). FEML dissociates the PDE modelling, which is tied to the system configuration considered, from the operator representing the missing physics, which is agnostic to system configurations and common across all physical systems that share the same physical properties (i.e., the hidden physics). Consequently, our framework naturally allows for zero-shot generalisation of complex physical systems that share the same hidden physics. It also enables downstream study of the learned model by domain specialists. Our framework uses structure-preserving operator networks (SPONs) to model the missing physics operator, which allows one to preserve key continuous properties at the discrete level, to learn over complex geometries and meshes, and to achieve zero-shot generalisation across different discretisations (i.e., different mesh resolutions and/or FE discretisations). We showcase our framework and its versatility by recovering nonlinear stress–strain laws from synthetic laboratory tests, applying the learned model to a new mechanical scenario without retraining, and identifying temperature-dependent conductivity in transient heat flow.

Introduction

Many science and engineering problems rest on well-understood physics yet contain unresolved or missing relationships that are unknown or cannot be readily expressed in mathematical form.

Modelling complex physical systems is traditionally achieved through physics-based models, such as partial differential equations (PDEs). However, such models require exact physical understanding and a fully specified mathematical formulation to accurately describe the physics of interest—conditions that are often difficult to satisfy in practice. Data-driven approaches, particularly machine learning (ML) models, offer an alternative by inferring input–output relationships directly from observable data, enabling prediction of system behaviour even when the governing physics are unknown or incomplete. However, purely data-driven models have their own drawbacks, including the need for large training datasets, predictive power limited to regimes represented in the training data, and reduced interpretability.

Various strategies have been proposed to incorporate physical and mathematical knowledge into machine-learning algorithms^{1–6}. In general, these approaches seek to address the shortcomings of purely data-driven models by training surrogate ML models with both data and physical constraints. Although this reduces the volume of data required, the resulting models typically learn the *solution of a particular PDE configuration* rather than the *unknown operator itself*.

*Email: ado.farsi@imperial.ac.uk

†Email: n.bouziani18@imperial.ac.uk. This work was conducted independently of Amazon.

‡Email: david.ham@imperial.ac.uk

In many applications, the missing physics does not correspond to an explicit input–output map, but rather manifests as an *internal operator*—a hidden functional relationship (such as a constitutive law or thermal material property) that governs interactions within the PDE system itself. This operator acts locally within the governing equations, coupling quantities (e.g., stresses or heat fluxes) through unknown dependencies that cannot be directly observed or isolated experimentally. Existing methods such as Fourier Neural Operators (FNO) or Physics-Informed Neural Operators (PINO)^{7,8} learn the full solution map from inputs to PDE solutions. In addition, they rely on pointwise discretisations of input–output fields that can discard the underlying continuous function-space structure, leading to inconsistencies and degraded operator approximation⁹. While effective as surrogate models, these approaches do not identify the hidden operator itself; instead, they approximate the entire configuration-specific mapping. Such approaches do not allow for learning missing physics operators that can then be reused across different problems, including problems with different discretisations, and provides little insight for scientific interpretation. The objective of the present work is instead to recover only the unknown relationship, such that (i) the learned operator can be transferred to other problem configurations, and (ii) the resulting model can be inspected and constrained by domain experts for downstream analysis. Learning such operators from data requires coupling traditional PDE solvers with machine learning models. Since the operator of interest is embedded within the PDE, measurable physical quantities, from which a training loss can be defined, can be obtained by solving the governing equations. This coupling necessitates *end-to-end differentiability* through both the PDE solver and the embedded ML operator, enabling gradients to propagate across the entire system during training².

In this work, we introduce Finite Element-Based Machine Learning (FEML), a general end-to-end differentiable framework for learning missing physics in systems with partially known governing laws. FEML cleanly separates known physics, expressed as PDEs in weak form and discretised with the finite element method (FEM), from unknown relationships, which are represented by ML operators embedded within the FEM solver. By embedding the PDE solver in the training loop and providing end-to-end differentiability, FEML enables learning from indirect measurements when operator inputs/outputs are not directly observable. Our framework employs *structure-preserving operator networks* (SPONs) to model the missing-physics operator. SPONs preserve key continuous properties at the discrete level, enable learning over complex geometries and meshes, and permit zero-shot generalisation across different discretisations (mesh resolutions and/or finite element choices). In addition, SPONs provide theoretical guarantees on operator approximation for a given training discretisation¹⁰.

The FEML framework is also particularly suited when some of the quantities involved in the unknown relationship are not directly measurable, allowing one to learn from data on related, measurable quantities within the same system. An example is the discovery of material constitutive models. Here, the unknown relationship is that between strains (i.e. material deformation) and stresses (the internal forces reacting to deformation); the latter, although it can be estimated under simplified loading conditions, is not directly measurable. The idea is to use known physical relationships to learn the constitutive model from measurable quantities such as displacements and applied forces (this will be covered in Section 1.2). One may then wish to examine the ML operator on its own to uncover the previously hidden relationships, for example by applying symbolic regression or sparse-identification techniques. In the context of constitutive modelling, this could enable the extrapolation of generalised stress–strain laws. One might also leverage the learned operator as a foundation model, trained on data from simplified laboratory tests, to predict material behaviour under different geometries and loading conditions without retraining (see Section 1.2.3). This has potential practical applications in many fields, such as subsurface engineering, where integrating sparse prior knowledge with limited field measurements is critical.

Our framework relies on Firedrake^{11,12} and allows for end-to-end differentiable coupling with ML architectures implemented in PyTorch¹³ and JAX¹⁴. To the best of our knowledge, the FEML framework is the first to support the bidirectional coupling of state-of-the-art general finite element solvers and arbitrary machine learning architectures in an end-to-end differentiable manner. In contrast, most existing efforts have focused on deploying the algorithmic differentiation pipelines of machine learning frameworks to yield differentiable physics constraints, often specialised to particular applications (such as *XLB*¹⁵, *PhiFlow*¹⁶, *Adept*¹⁷). A similar approach to ours has been presented in¹⁸, although it lacks the adjoint capabilities required for differentiation through constraints based on PDEs, and in⁴, although it is limited to a restricted set of fluid simulations.

This work is organised as follows. Section 1.1 presents our FEML framework for learning missing physics by embedding trainable ML operators within PDE systems. Section 1.2 illustrates its application to solid mechanics. Section 1.3 extends the examples to transient thermodynamics by learning nonlinear thermal conductivities from noisy temperature fields. These examples are designed to increase in complexity to progressively build intuition for the proposed framework, from an initial setting with simple geometry and boundary/loading conditions to a final case involving a complex multi-component domain and a time-dependent governing equation with fluctuating boundary conditions. Finally, Section 2 summarises our findings and outlines directions for future work. The code required to reproduce all examples presented herein is available in a companion repository.

1 Results

1.1 Framework

We introduce the Finite Element-Based Machine Learning (FEML) framework, a general and end-to-end differentiable approach for learning missing physics, that is, unknown relationships between quantities in systems where partial physical knowledge is available. Our main motivation is to learn operators that model such unknown relations. We consider an operator $\mathcal{G} : \mathcal{U} \rightarrow \mathcal{V}$, where \mathcal{U} and \mathcal{V} are (typically infinite-dimensional) Hilbert spaces of functions defined on a bounded domain $\Omega \subset \mathbb{R}^d$ in spatial dimension $d \in \{1, 2, 3\}$. For sake of simplicity, we consider \mathcal{U} and \mathcal{V} to be defined on the same domain Ω , but different bounded domains and spatial dimensions can be considered. We introduce a framework for approximating \mathcal{G} by a learnable operator $\mathcal{G}_\theta : \mathcal{U}_h \rightarrow \mathcal{V}_h$ of parameters θ , where \mathcal{U}_h and \mathcal{V}_h are finite element spaces arising from the discretisation of the spaces \mathcal{U} and \mathcal{V} , respectively.

Such operators can traditionally be learned in a supervised manner from direct observations, i.e. a set of input-output pairs $\{(x_i, \mathcal{G}(x_i))\}_i$, with $x_i \in \mathcal{U}$. However, in practice, many input–output signals from unknown operators cannot be accessed directly via experiments, since they form only part of a larger physical model governed by a PDE and consequently, we cannot learn them directly. For example, constitutive models describing the stress-strain relationship of a material are generally unknown, and the resulting stress tensor, which encodes internal forces under deformation, cannot be measured directly. In contrast, the displacement field is measurable and satisfies a PDE that incorporates this constitutive relation. Therefore, to learn the constitutive model, we embed our ML model within the PDE solver: during training, the ML model predicts the stress tensor required by the solver to compute the corresponding displacement, and we compute a loss against the measured displacement to update the model.

Our aim is to learn \mathcal{G}_θ under some loss $\mathcal{L}(u_\theta, u^{obs})$, where u_θ is a PDE solution and u^{obs} are observable data, i.e. we have:

$$F(u_\theta, \mathcal{G}_\theta(u_\theta); v) = 0 \quad \forall v \in U_h \quad (1)$$

where (1) is the variational form of the PDE with F the residual. This PDE can be linear or non linear, steady or time-dependent. In practice, one can also equip it with boundary conditions but we have simplified the setup description for sake of simplicity.

We propose a general framework and the loss function \mathcal{L} can be defined in different ways depending on the specific problem. Figure 1 shows a schematic of the proposed framework. For example, in the case of learning a constitutive model in Section 1.2.2, F is the residual of the PDE that describes the equilibrium equation with some boundary conditions in the simulated domain. Moreover, \mathcal{L} quantifies the discrepancy between experimental displacement measurements and the corresponding solution of the FEM solver, and \mathcal{G}_θ is an unknown constitutive law.

Our framework combines PDE modelling of the physical problem of interest with ML modelling of the operator to approximate. Minimising the loss $\mathcal{L}(u_\theta, u^{obs})$ for training requires computing the gradient of the loss with respect to the parameters, i.e. $\frac{d\mathcal{L}}{d\theta}$, which by chain rule requires the gradient of the PDE solution with respect to the parameters, i.e. $\frac{du_\theta}{d\theta}$, which in turn necessitates the gradient of the ML operator, i.e. $\frac{d\mathcal{G}_\theta}{d\theta}$. In other words, learning \mathcal{G}_θ requires end-to-end differentiability of the entire system, i.e. being able to differentiate through the PDE solution u_θ and through the ML components of the system to compute $\frac{d\mathcal{L}}{d\theta}$.

Many real-world problems and engineering applications require the use of advanced numerics with state-of-the-art capabilities for PDE modelling. The simulation of complex physical systems by coupling advanced numerics for PDEs with state-of-the-art machine learning demands the composition of specialist PDE solving frameworks with industry standard machine learning tools. Hand-rolling either the PDE solver or the ML model will not cut it. Our framework introduces a generic differentiable programming interface that allows to combine the state-of-the-art Firedrake framework for PDE modelling, with different ML frameworks, including PyTorch¹³ and JAX¹⁴ deep learning libraries. As a result, it provides scientists and engineers with an efficient and highly productive way to learn operators combining FEM operations, e.g. solving a PDE using FEM, with ML algorithms, thanks to end-to-end differentiability and benefiting from state-of-the-art performance of both FEM and ML libraries.

1.1.1 Operator Learning over Finite Element Spaces

Our framework differs from the traditional operator learning literature as it embeds the learnable operator \mathcal{G}_θ into a differentiable FEM solver, thereby allowing end-to-end differentiable FEM-based operator learning. Another notable difference is that our setting entails learning over finite element spaces, i.e. \mathcal{U}_h and \mathcal{V}_h result from finite element discretisations. Consequently, the operator \mathcal{G}_θ can be expressed as an encode-process-decode architecture¹⁰, with a learnable processor over the spaces induced by the degrees of freedom (DoF) of \mathcal{U}_h and \mathcal{V}_h . More precisely, \mathcal{G}_θ can be defined as

$$\mathcal{G}_\theta(f) = \mathcal{D} \circ \mathcal{P}_\theta \circ \mathcal{E}(f), \quad f \in \mathcal{U}_h, \quad (2)$$

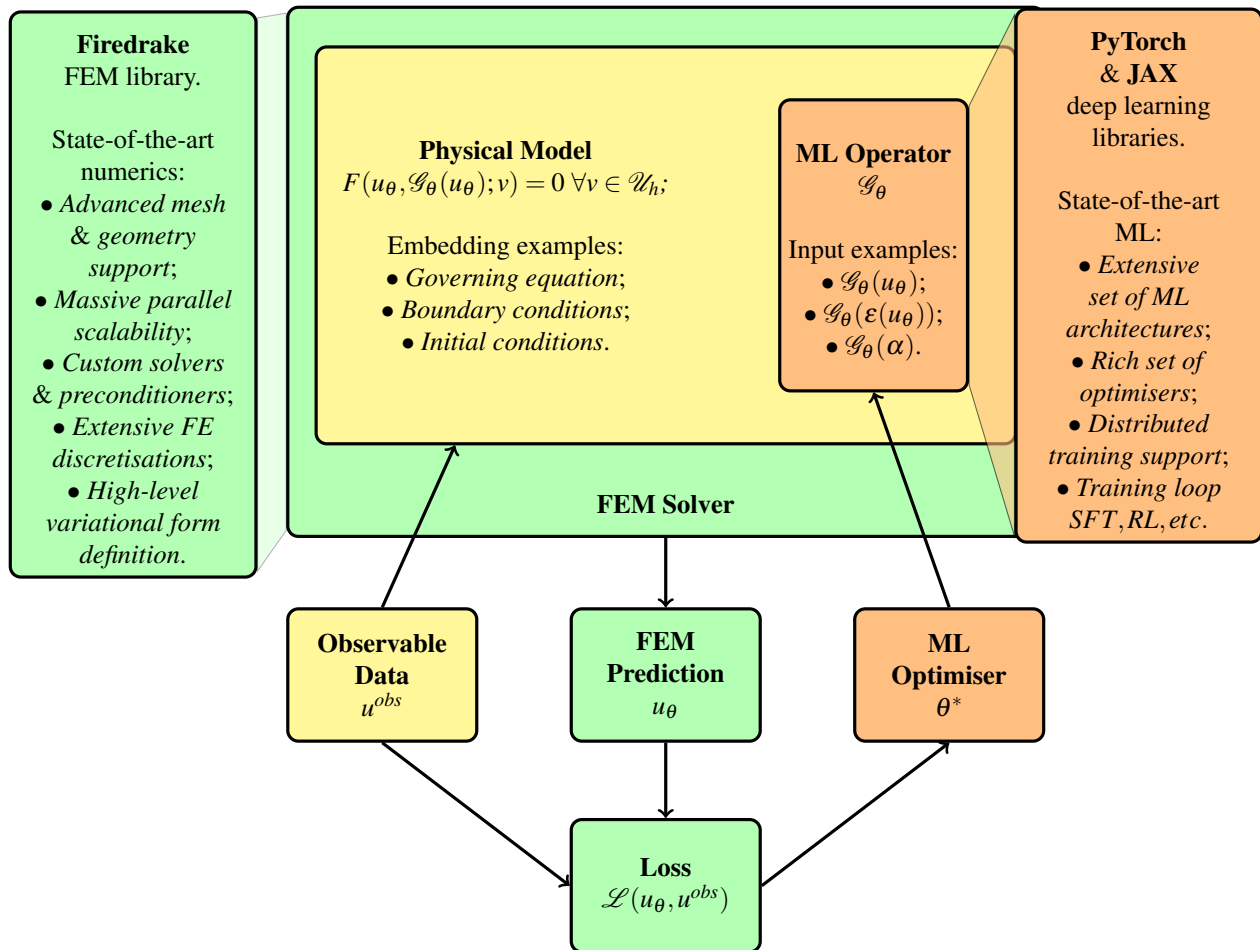


Figure 1. Schematic of the proposed framework for embedding neural networks as trainable operators within PDE systems. The framework combines finite element solvers with machine learning models to learn ML operators from observable data.

where \mathcal{E} and \mathcal{D} refer to the *encoder* and *decoder*, while $\mathcal{P}_\theta: \mathbb{R}^n \mapsto \mathbb{R}^m$ with $n = \dim(\mathcal{U}_h)$ and $m = \dim(\mathcal{V}_h)$ represents a learnable model of parameters θ , known as the *processor*. The encoder extracts the degrees of freedom of an input function $f \in \mathcal{U}_h$:

$$\mathcal{E}(f) = (f_1, \dots, f_n), \quad (3)$$

where $f_i = \langle f, \phi_i \rangle$ corresponds to the Galerkin projection onto the i -th basis function ϕ_i . On the other hand, the decoder maps the predicted DoFs in \mathcal{V}_h to the reconstructed solution $u \in \mathcal{V}_h$ as

$$\mathcal{D}(u_1, \dots, u_m) = u, \quad (4)$$

with $u(x) = \sum_{i=1}^m u_i \phi_i(x)$, for $x \in \Omega$, and where $(\phi_i)_{1 \leq i \leq m}$ a basis of \mathcal{V}_h . Such encode-process-decode operators are referred to as *structure-preserving operator networks* (SPON)¹⁰ as they preserve some key mathematical and physical properties of the operator \mathcal{G} at the discrete level and offer explicit trade-off between accuracy and efficiency. Our framework inherits the properties of SPON such as zero-shot super-resolution and theoretical bounds on the approximation error of \mathcal{G}_θ .

Zero-shot super resolution. \mathcal{G}_θ outputs a finite element function $u \in \mathcal{V}_h$ that can be evaluated at any point x in the geometrical domain Ω , i.e. by simply using $u(x) = \sum_{i=1}^m u_i \phi_i(x)$. This property results from the FE discretisation of \mathcal{U} and \mathcal{V} and holds on complex geometries and independently of the mesh and resolution \mathcal{G}_θ was trained on. This relation is crucial for transferring solutions between different meshes and spatial discretisations, such as for zero-shot super-resolution, and it enables architectures that can seamlessly operate across multiple resolutions. In practice, implementing such a property for complex geometries and/or non-trivial FE discretisations is challenging. However, our differentiable programming coupling of Firedrake and ML software allows to implement that in a single line of code for arbitrary meshes and a wide range of FE discretisations.

Approximation error. Let Ω be an open bounded domain of \mathbb{R}^n , $\mathcal{V} = H^k(\Omega)$ and $\mathcal{U} \subset H^k(\Omega)$. Let $\mathcal{G}: H^s(\Omega) \rightarrow \mathcal{V}$ be a Lipschitz continuous operator for some $0 \leq s \leq k$ and $0 < \varepsilon < 1$, and \mathcal{U}_h and \mathcal{V}_h be conforming finite element spaces. Under mild assumption on \mathcal{U} and assuming \mathcal{U}_h and \mathcal{V}_h satisfy the standard finite element hypotheses¹⁹, one can show that there exists a learnable operator $\mathcal{G}_\theta: \mathcal{U}_h \rightarrow \mathcal{V}_h \subset \mathcal{V}$ with a number of parameters bounded

$$|\theta| < C_1 \varepsilon^{-C_2/h^{k^n}} (\log(1/\varepsilon) + 1),$$

such that for all $f \in \mathcal{U}$,

$$\|(\mathcal{G} - \mathcal{G}_\theta \circ P_{\mathcal{U}})(f)\|_{H^s(\Omega)} \leq C_3 h^{k-s} \left(\|f\|_{H^k(\Omega)} + \|\mathcal{G}(f)\|_{H^k(\Omega)} \right) + \varepsilon(h), \quad (5)$$

where $P_{\mathcal{U}}: \mathcal{U} \rightarrow \mathcal{U}_h$ is the Galerkin interpolation. We refer to¹⁰ for the general approximation theorem and its proof. The first term denotes the finite element error on the input-output spaces, which can be controlled via the finite element discretisation, e.g. a higher polynomial degree k results in a higher convergence rate via h^{k-s} . On the other hand, the second term translates the quality of the neural network approximation as the number of parameters increases. The left-hand side in eq. (5) can be seen as an operator aliasing error⁹, which can be explicitly controlled by the mesh resolution and the discretisation of the input-output spaces. It is worth noting that higher-order discretisations comes with higher convergence rate but also with an additional computational cost as it increases the number of DoFs and therefore the size of the input-output of the learnable processor \mathcal{G}_θ . This trade-off between accuracy and efficiency is well known in the FEM literature and is inherited by our framework.

In the following sections, we present examples of the proposed framework applied to solid mechanics and thermodynamics. Section 1.2 focuses on learning non-linear constitutive models, while Section 1.3 demonstrates the learning of non-linear thermal properties in transient heat conduction problems.

1.2 Learning Materials Constitutive Models

In this section, we demonstrate the application of the proposed framework to solid mechanics and materials science. Different materials exhibit different deformation behaviours under applied forces. For instance, the relationship between deformation and the internal forces can varies significantly when studying rocks, metals, or other engineered metamaterials. Accurately characterising these relationships is crucial in many engineering domains, from the design of resilient infrastructure in civil engineering to the development of aircraft structures in aeronautical engineering. We present two examples in which non-linear constitutive models are implemented using ML models.

Two ML constitutive models are trained on distinct datasets to illustrate the versatility of the proposed framework. The pre-trained model is then employed as a foundation model and applied via zero shot inference to a novel problem with increased dimensionality from two to three dimensions, together with altered geometries and loading conditions compared with those used during training. This demonstrates the transferability and robustness of the learned operators as generalised constitutive components within a foundation modelling framework.

The formulation of the solid mechanics problem with the embedded ML constitutive model is detailed in Section 3.1. An ML constitutive model is trained using loads obtained from displacement-controlled tests in Section 1.2.1 and displacements from load-controlled tests in Section 1.2.2. In Section 1.2.3 the trained constitutive ML model is then used to simulate a higher-dimensional problem (from 2D to 3D) and different boundary conditions, demonstrating the generality and robustness of the proposed framework to be used for zero shot inference in foundation models.

1.2.1 Learning from Loads in Displacement-Controlled Experiments

In this subsection, we focus on displacement-controlled uniaxial tests—standard experiments in materials science, rock mechanics, and civil engineering to assess the compressibility and strength of materials.

We idealise the sample as a 2D rectangular domain, as depicted in Figure 2. The two vertical sides of the sample are free, while the bottom and top surfaces have imposed displacements. The bottom surface is fixed throughout the simulation. A prescribed displacement \bar{u}_i is applied to the top surface, where i is an integer from 1 to N that represents the sequence of displacements applied during the experiment. This configuration simulates the quasi-static loading condition in which time increments correspond to sequential deformation steps rather than physical time. Figure 3 illustrates the mathematical definition of the problem and the proposed framework for learning constitutive models from displacement-controlled experiments.

The loss function is computed as:

$$\mathcal{L} = \frac{1}{N} \sum_i^N \frac{|F_i^{\text{fem}} - F_i^{\text{obs}}|}{|F_i^{\text{obs}}|} \quad (6)$$

where F_i^{fem} is the applied load predicted by the FEM model with the ML-based constitutive model at time step i , and F_i^{obs} is the corresponding synthetic experimental load. It is important to note that the poisson effects are not taken into account in this definition of the loss function and therefore the constitutive model is not univocally defined. In this example, we are assuming that the poisson effects are described by a Poisson's ratio of 0.3. This assumption is relaxed in the next example, since the displacement field allows to univocally define the constitutive model. More details about the more general architecture of the ML constitutive model and the symmetries imposed by physical constraints are described in detail in Section 3.1.2.

The synthetic experimental data is generated by solving the same PDE system with a known constitutive model, in this case a non-linear softening law. The training dataset consists of six force-displacement pairs, with four additional pairs used for model validation. To represent real data, a 1% noise is added to the synthetic experimental data.

Figure 4 shows the training and validation loss curves together with the evolution of the force–displacement response predicted by the FEM solver incorporating the ML-based constitutive model at successive training stages (epochs 10, 20, and 200). The dotted line denotes the reference force–displacement curve, while the red line indicates the model prediction. After 10 and 20 epochs, the ML-based model captures an almost linear elastic response. After 200 epochs, it accurately reproduces the material's softening behaviour, demonstrating its ability to learn general nonlinear constitutive responses from a minimal training dataset.

1.2.2 Learning from Displacements in Load-Controlled Experiments

In this section, we consider the *Brazilian disc test*, a standard method widely used in engineering to indirectly measure the tensile strength of materials. During the test, the displacement field is typically recorded using digital image correlation²⁰. The experiment is performed under force control, where the applied load \bar{F}_i is prescribed rather than the displacement.

In this example, the sample is idealised as a 2D circular disc, as shown in Figure 5. The bottom of the disc is fixed throughout the simulation, while a force \bar{F}_i is applied at the top of the sample, where i is an integer from 1 to N that represents the sequence of forces applied during the test. Similarly to the previous example, this configuration simulates the quasi-static loading condition in which time increments correspond to sequential loading steps rather than physical time.

Figure 6 illustrates the mathematical definition of the problem and the proposed framework for learning constitutive models from load-controlled experiments. The parameters of the neural network-based constitutive model are learned by minimising the following loss function:

$$\mathcal{L} = \frac{1}{N} \sum_i^N \frac{|u_i^{\text{fem}} - u_i^{\text{obs}}|}{|u_i^{\text{obs}}|}, \quad (7)$$

where u_i^{fem} represents the displacement field predicted by the FEM solver with the ML-based constitutive model at loading step i , and u_i^{obs} is the corresponding synthetic experimental displacement field.

The synthetic experimental data is generated by solving the same PDE system with a known constitutive model. As in the previous example, we use a non-linear softening law. The training dataset consists of 4 force-displacement field pairs, with 3

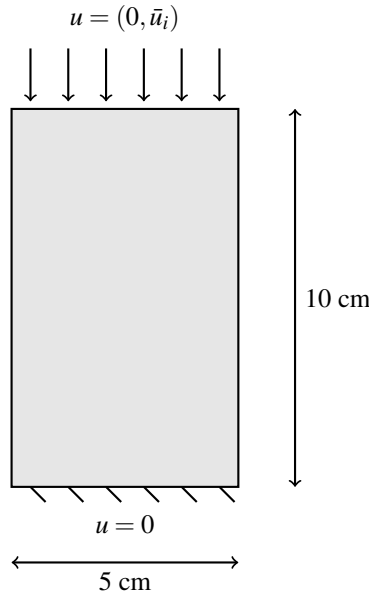


Figure 2. Schematic of the 2D displacement-controlled uniaxial test. The rectangular sample has free vertical boundaries, a fixed bottom, and a prescribed displacement \bar{u}_i applied at the top.

additional pairs used for model validation. To represent real data, a 1% noise is added to the displacement fields in the synthetic experimental data.

Figure 7 illustrates the training and test loss curves (continuous and dashed lines, respectively). The figure also shows a comparison corresponding to the maximum load in the test dataset: the final deformed shape (amplified for clarity), and the displacement magnitude field predicted by the FEM solver incorporating the ML-based constitutive model at training epochs 10 and 100. The dotted outline represents the reference (ground truth) deformation and the red line is the deformation prediction. Initially, due to the universal approximation properties of MLs, the model overestimates deformations under applied loads (epoch 10), progressively improving its accuracy. By epoch 100, the ML-based constitutive model closely matches the reference deformation, benefiting from the richer training data comprising nodal displacement fields at four load increments. Compared to the previous example, the loss exhibits a more consistent decrease, which can be attributed to the increased amount of training data. While the prior case relied on only six scalar force-displacement pairs, here, each training step includes nodal displacement fields, providing significantly more information. Given the complexity of the sample's deformation profile, each node undergoes a distinct strain-stress state, enriching the training dataset and enhancing the constraints on the ML-based constitutive model.

1.2.3 Zero Shot Inference with a Foundation Model

We demonstrate the portability of our pretrained constitutive model by deploying it zero-shot on a problem that differs from the training setup. We treat the constitutive operator as a part of a foundation model: a reusable, data-driven component pretrained once and then inserted into new simulations without retraining or architectural changes, while allowing modifications to the surrounding governing PDEs, geometry, and/or boundary/initial conditions.

The constitutive model was trained under the simplified loading conditions of the Brazilian disc test (diametral compression; see Section 1.2.2). Here, we apply the same model directly to a three-dimensional plate with a central hole subjected to torsion. As shown in Figure 8, the lower face is fixed and a rotation of $\theta = 1^\circ$ is prescribed on the upper face, producing a strongly heterogeneous stress field around the perforation and through the thickness.

The finite element formulation is summarized in Figure 9. Standard FEM provides the kinematics, balance laws, and boundary/loading conditions. The pretrained constitutive operator supplies the stress response from the computed strain field, thereby closing the system without additional calibration.

Figure 10 compares the resulting mean stress distribution with the reference solution generated by the synthetic ground-truth constitutive law. The close agreement indicates that the learned operator transfers to a new geometry, three-dimensional setting, and loading regime in a zero-shot manner. This portability highlights the utility of embedding pretrained operators within PDE solvers to enable efficient simulation across varied engineering scenarios.

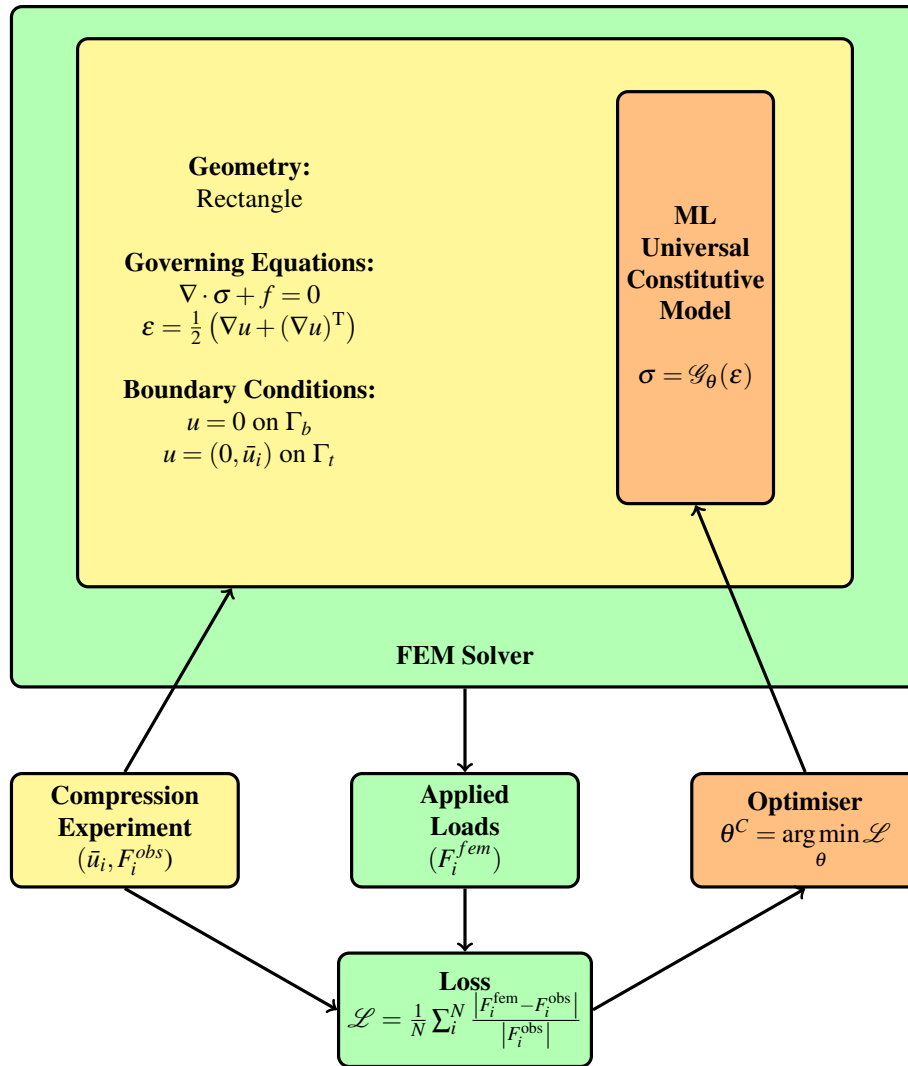


Figure 3. Schematic of the mathematical definition of the problem and the proposed framework for learning constitutive models from displacement-controlled experiments.

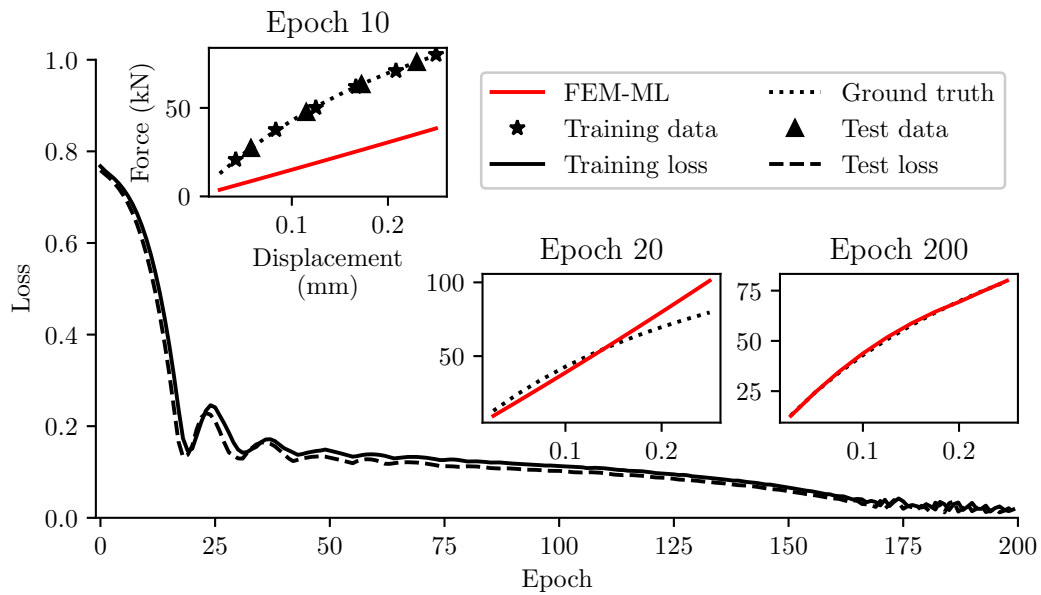


Figure 4. Training loss curve and force-displacement response at different training stages. The figure presents the training and test loss curve alongside the force-displacement response predicted by the FEM solver incorporating the ML-based constitutive model at training epochs 10, 20, and 200. In the plot corresponding to epoch 10, star markers denote the six force-displacement data points used for training, and triangle markers denote the 4 values used for model validation (test). The dotted line represents the reference (ground truth) force-displacement curve, while the red line corresponds to the response predicted by the FEM solver employing the learned constitutive model. Owing to the universal approximation properties of MLs, the model initially approximates the material behaviour as an almost linear elastic response (epoch 10 and 20). After 200 epochs, the ML-based constitutive model accurately captures the softening behaviour of the material, achieving a close match to the reference curve despite being trained on only six data points.

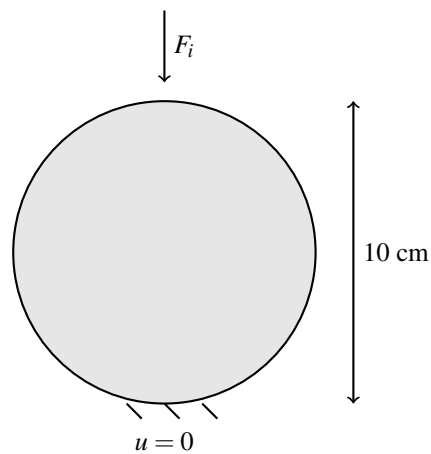


Figure 5. Schematic of the Brazilian disc test. The sample is represented as a circular disc with a fixed bottom and a prescribed time-dependent force $F(t)$ applied at the top.

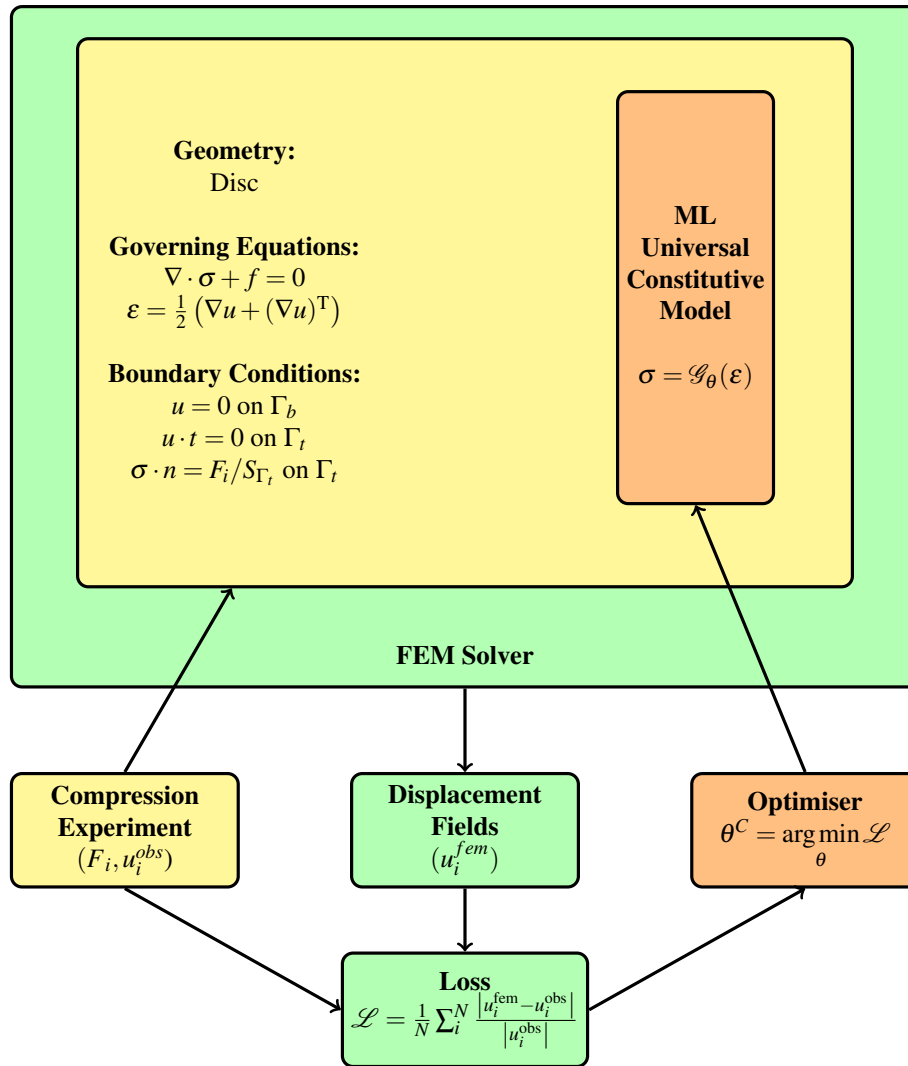


Figure 6. Schematic of the mathematical definition of the problem and the proposed framework for learning constitutive models from load-controlled experiments.

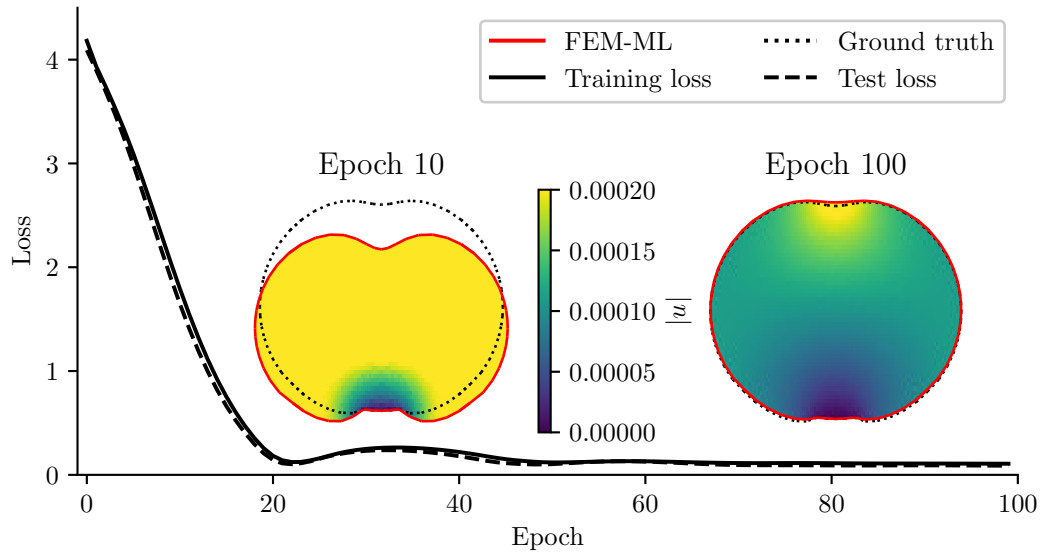


Figure 7. Training loss curve, final deformation, and displacement magnitude field at different training stages. The figure presents the training and test loss curves (continuous and dashed line respectively). The figure also show a comparison of the results for the maximum test load data with the final deformed shape (amplified for visualisation) and the displacement magnitude field predicted by the FEM solver incorporating the ML-based constitutive model at training epochs 10 and 100. The dotted line represents the reference (ground truth) deformation and the red line is the deformation prediction. Initially, due to the universal approximation properties of MLs, the model overestimates deformations under applied loads (epoch 10), progressively improving its accuracy. After 100 epochs, the ML-based model closely matches the reference deformation, benefiting from the richer training data comprising nodal displacement fields at four load increments.

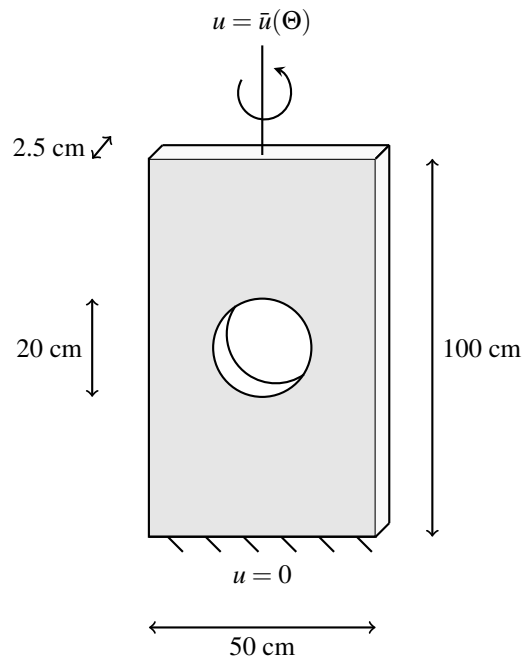


Figure 8. Schematic of the 3D plate with a central hole subjected to a 1° rotation at the top edge. The plate is fixed at the bottom.

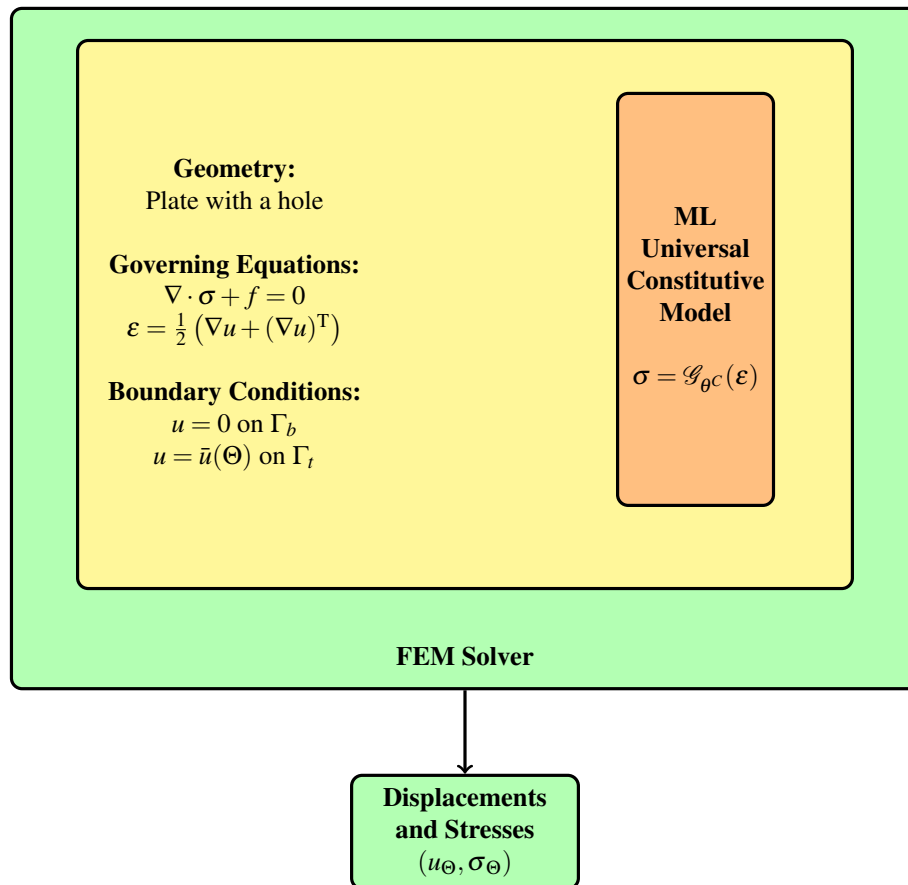


Figure 9. Schematic of the foundation model with the pretrained constitutive operator for zero shot transfer to a three dimensional plate with a central hole under torsional loading.

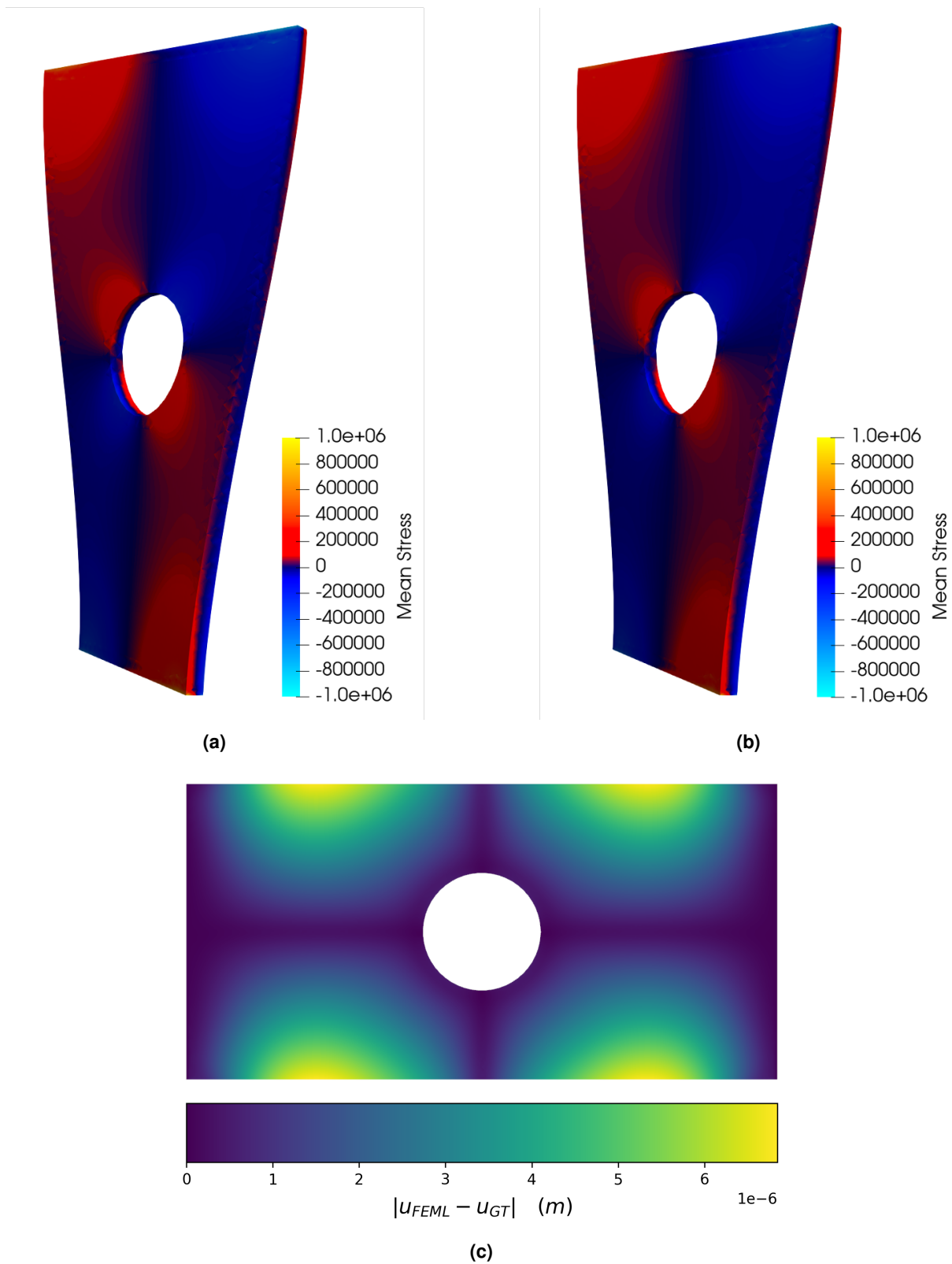


Figure 10. Comparison of mean stress distributions: (a) results from the foundation model with the trained ML-based constitutive model, and (b) results from the synthetic ground truth model. The deformations have been amplified for visualisation purposes. (c) Magnitude of the absolute error between the displacements calculated with the ML-based constitutive model and with the synthetic ground truth model. The maximum error is 3 order of magnitude smaller than the maximum displacement.

1.3 Learning in Transient Thermodynamics Problems

In this section, we showcase the application of the proposed framework to transient thermodynamics problems, focusing on the learning of non-linear thermal properties. Many materials exhibit temperature-dependent thermal behaviour, which significantly influences heat transfer processes. For instance, rocks, and ceramics respond differently to temperature variations, affecting their thermal performance in geothermal applications, civil engineering applications like bridge thermal expansion analysis, and ceramics, including high-temperature industrial reactors. Capturing these non-linear thermal properties is essential for accurate simulations and predictive modelling.

The formulation of the transient thermodynamics problem is detailed in Section 3.2. In the following sections, we show how the proposed framework can be used to learn the non-linear thermal properties of the square plate from temperature measurements.

1.3.1 Learning Thermal Properties from Temperature Measurements

In this example, we consider a transient heat conduction problem on two bodies: a copper disc and a square plate, as shown in Figure 11(a). The copper disc is assumed to have a known constant thermal conductivity, while the square plate has an unknown thermal conductivity that is a non-linear function of temperature which is parametrised with an ML model.

The two bodies start at room temperature, and then a heat source is applied to the left side of the copper disc, highlighted in dark gray. The heat source generates a fluctuating temperature boundary condition \bar{T}_i that increases in amplitude over time. The temperature field of the square plate is then measured at different times i . Figure 11(b) shows the temperature field at the end of the experiment. The mathematical definition of the problem is illustrated in Figure 12.

The loss function used to train the ML model is defined as:

$$\mathcal{L} = \frac{1}{N} \sum_i^N \frac{|T_i^{\text{fem}} - T_i^{\text{obs}}|}{|T_i^{\text{obs}}|}, \quad (8)$$

where T_i^{fem} represents the temperature field predicted by the FEM solver with the non-linear ML thermal conductivity model at time step i , and T_i^{obs} is the corresponding synthetic experimental temperature field. The synthetic experimental data is generated by solving the same PDE system with a known non-linear thermal conductivity model. Both the training and test datasets consist of temperature fields at 12 time steps, but the two datasets are generated from two different synthetic experiments with different temperature boundary conditions. A 2% noise is added to the temperature fields in the synthetic experimental data to represent real data.

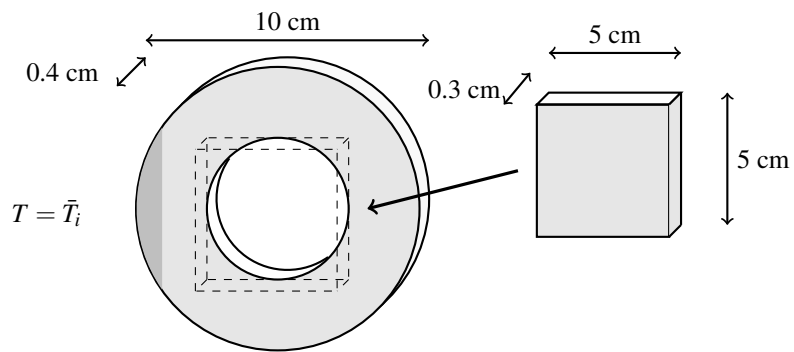
Figure 13 shows the evolution of the training and test loss, as well as the thermal conductivity profile predicted by the machine learning model embedded in the FEM solver, evaluated at epochs 10, 50 and 100. The dotted line represents the reference thermal conductivity model, which exhibits a non-linear dependence on temperature, while the red line shows the corresponding predictions from the ML model. At early stages of training (e.g. epoch 10), the model fails to capture the correct trend and deviates significantly from the ground truth. By epoch 50, the learned conductivity shows partial agreement, although noticeable discrepancies remain. After 150 epochs, the ML-based model successfully reproduces the non-linear thermal response, closely matching the reference profile across the entire temperature range. This highlights the model’s ability to progressively learn the underlying physical law through training.

2 Discussion and Conclusions

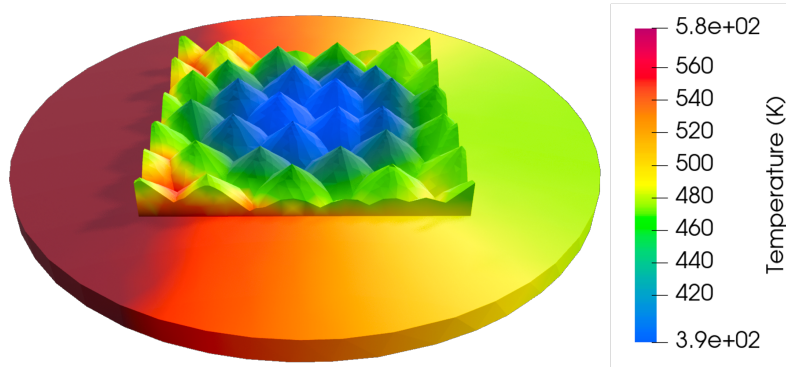
We have introduced FEML, a fully differentiable finite element–based machine learning framework for discovering missing physics in systems governed by partial differential equations. The key idea is to retain the known governing equations in their standard finite element (FEM) form, while representing the unknown physical relationships as trainable operators embedded within the variational formulation. By differentiating end-to-end through both the FEM solver and the machine learning components, FEML enables the identification of internal operators—such as constitutive or transport laws—from indirect, experimentally accessible quantities. In contrast to surrogate models that learn configuration-specific PDE solutions, the learned operator in FEML is defined on function spaces and can be reused across geometries, boundary conditions, dimensions, and discretisations.

A central ingredient of the framework is the use of structure-preserving operator networks (SPONs) to parameterise the missing-physics operator. By operating on the degrees of freedom of finite element spaces, SPONs preserve key properties of the continuous operators at the discrete level, and come with theoretical guarantees. SPON models offer zero-shot cross-discretisation capabilities, which we demonstrated on our numerical experiments: once trained, the operator can be evaluated on meshes and finite element spaces different from those used during training, without additional retraining.

We assessed FEML on a sequence of solid mechanics problems in which the hidden operator is a nonlinear constitutive relation. In the displacement-controlled uniaxial test, FEML recovered a nonlinear softening law from a noisy and extremely



(a)



(b)

Figure 11. (a) Schematic of the problem showing a disc-shaped copper plate (diameter 10 cm, thickness 0.4 cm, central hole diameter 5 cm) with a square plate of edge 5 cm with an irregular roughness and average thickness 0.3 cm. (b) displays the corresponding temperature distribution.

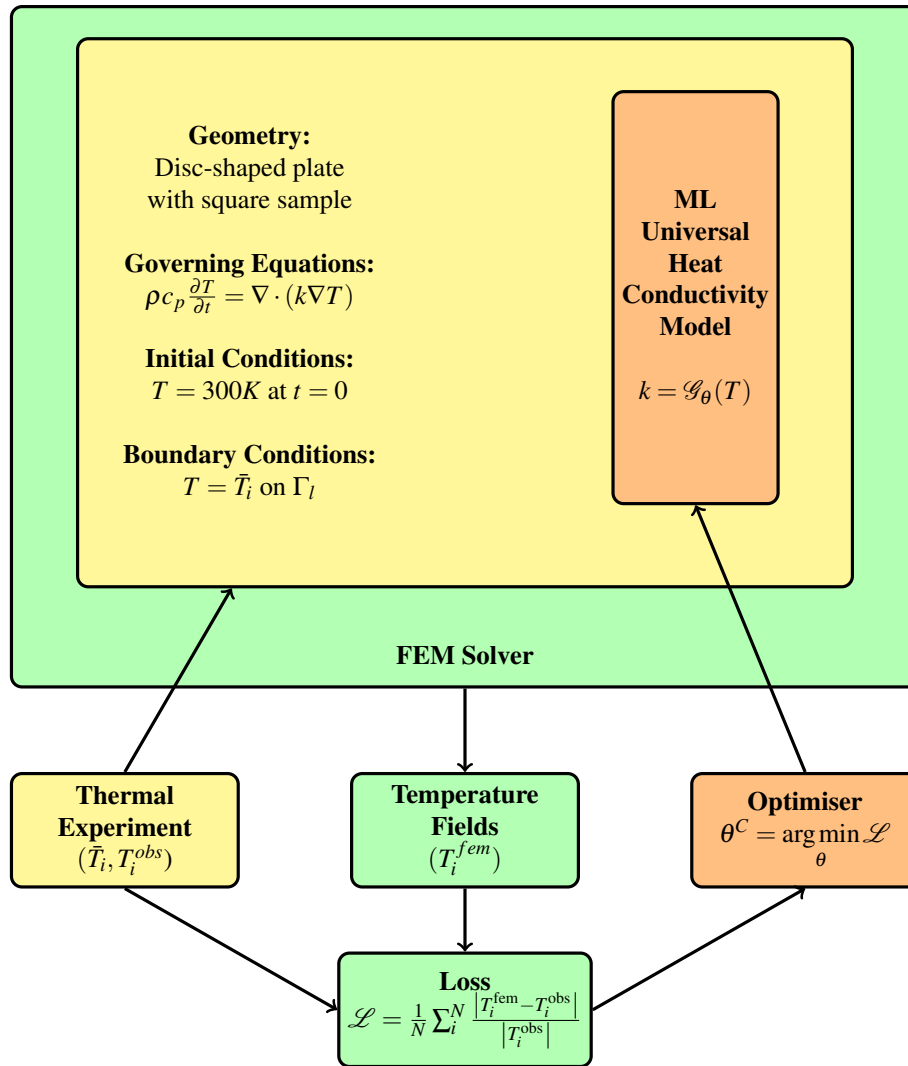


Figure 12. Schematic of the mathematical formulation of the transient heat conduction problem and the proposed framework for learning thermal properties from temperature measurements.

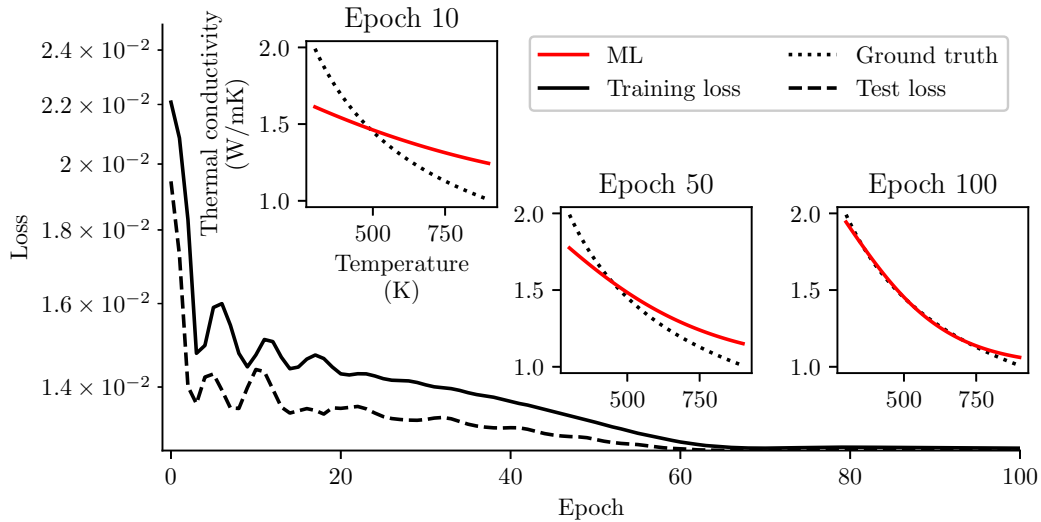


Figure 13. Training and test loss curves are shown alongside the thermal conductivity as a function of temperature for the machine learning model integrated within the FEM solver. Results are presented for training epochs 10, 50 and 100. The dotted line indicates the reference thermal conductivity model (ground truth), while the red line represents the relationship learned by the ML model. By epoch 100 the model accurately captures the non-linear dependence of thermal conductivity on temperature observed in the reference model.

sparse dataset: just six force–displacement values, perturbed with 1% noise. Despite having access only to global load measurements, and no direct stress information, the learned operator reconstructed the full stress–strain response closely matching the reference behaviour. This illustrates both the data efficiency of the framework and the advantage of exploiting equilibrium constraints through the embedded FEM solver.

In the load-controlled Brazilian disc example, the framework leveraged full-field displacement data to identify a more richly constrained constitutive model. The learned operator reproduced complex deformation fields under indirect loading when trained on noisy nodal displacement fields at only a few load levels. Compared with the uniaxial test, this setting corresponds to a regime where each node explores a distinct local strain state, providing a diverse collection of strain–stress conditions from which the operator can be inferred. In both solid mechanics cases, embedding the ML operator into the FEM solver allowed the model to exploit equilibrium and compatibility, thereby improving data efficiency and physical consistency relative to purely data-driven surrogates.

We then used the trained constitutive model operator in a foundation model and applied it in a zero-shot fashion to a three-dimensional plate with a central hole under torsion. Without any retraining, the learned operator produced displacement and stress fields in close agreement with the reference solution, with the relative error in the maximum displacement on the order of 10^{-3} (approximately 0.1%). This level of accuracy is noteworthy given that the operator was trained on noisy data from a different mechanical test (a two-dimensional load-controlled compression experiment on a disc) and then transferred to a 3D geometry, with different loading and boundary conditions. This result illustrates a main advantage of operator-level learning over solution-level surrogates: once the hidden physics has been identified, the same operator can be deployed as a reusable component in new scenarios, rather than being restricted to the configuration on which it was trained.

To demonstrate FEM applications beyond quasi-static solid mechanics, we apply the framework to a transient heat-conduction problem in which the missing physics is an unknown temperature-dependent thermal conductivity. The operator was trained from noisy temperature fields (with 2% perturbations) measured on a heterogeneous, coupled 3D geometry comprising a copper disc and an irregular square plate. The learned thermal law accurately reproduced the underlying nonlinear conductivity profile and generalised to a test experiment with different temperature boundary conditions. This example demonstrates that the framework extends naturally to time-dependent problems and heterogeneous materials, and that it can accommodate realistic levels of measurement noise in complex three-dimensional configurations.

The present work also suggests several opportunities and limitations that warrant further investigation. First, although end-to-end differentiability through a mature FEM stack enables flexible model discovery, it comes at a computational cost: repeated adjoint solves over large meshes can be expensive, particularly in three-dimensional, highly nonlinear, or multiphysics settings. Efficient solvers, reduced-order models, and mixed-precision or multi-fidelity training strategies will be important to scale FEM to field-scale applications. Second, identifiability issues can arise when multiple operators or parameters produce

similar observables; addressing this will require careful experiment design, regularisation informed by prior knowledge, and possibly multi-modal data.

Future work that goes beyond direct physics discovery, will include the use of FEML in a surrogate-modelling, where the embedded ML operator emulates expensive high-order coupling terms in a full-order PDE model. In such a workflow, high-fidelity simulations provide training data for the operator, which then replaces the costly components in subsequent simulations. This strategy has the potential to deliver reduced-order models that retain the fidelity of the original FEM formulation while significantly lowering computational cost, with applications ranging from nonlinear constitutive modelling and fracture to multiphase flow and thermomechanical coupling.

In summary, FEML provides a general and flexible route to combine physics-based finite element solvers with data-driven operator learning. By preserving known physics, learning only the missing relations, and respecting the underlying function-space structure, the framework yields data-efficient and interpretable operators that can be ported across problems, geometries, and discretisations. We expect this combination of differentiable PDE solvers and structure-preserving operator networks to underpin a new class of predictive tools for computational solid mechanics, thermodynamics, and, more broadly, for scientific and engineering applications in which incomplete physical knowledge must be reconciled with limited but informative data.

3 Methods

3.1 Solid mechanics problem formulation

We consider a quasi-static problem in the small displacement regime, described by a time-independent system of partial differential equations (PDEs) that includes the conservation of linear momentum and the constitutive relation between stress and strain. The governing equations are as follows:

$$\nabla \cdot \boldsymbol{\sigma} + f = 0, \quad (9)$$

where $\boldsymbol{\sigma}$ (N/m²) is the stress tensor and f (N/m³) represents body forces, which are assumed to be zero in this example. The kinematic relation between the displacement field u and the strain tensor $\boldsymbol{\varepsilon}$ is given by

$$\boldsymbol{\varepsilon} = \frac{1}{2} (\nabla u + (\nabla u)^T), \quad (10)$$

where u (m) is the displacement field and $\boldsymbol{\varepsilon}$ is dimensionless.

A nonlinear constitutive relation between the strain tensor $\boldsymbol{\varepsilon}$ and the stress tensor $\boldsymbol{\sigma}$, parameterised by the ML model:

$$\boldsymbol{\sigma} = \mathcal{G}_\theta(\boldsymbol{\varepsilon}), \quad (11)$$

where \mathcal{G}_θ denotes an operator with a neural network with learnable parameters θ .

3.1.1 Simulating Displacement-Controlled Uniaxial Experiments

The specimen simulated in Section 1.2.1 is a discretised with a triangular mesh, as shown in Figure 14a. The displacement field is approximated with cubic polynomial basis functions. The ground truth constitutive law is a nonlinear function of the strain tensor: the Poisson's ratio is fixed to a value of $\nu = 0.3$, while the Young's modulus is defined with:

$$E = c_1 \frac{1}{1 + c_2 |\text{tr}(\boldsymbol{\varepsilon}(u))|} \quad (12)$$

where $c_1 = 10^9$ and $c_2 = 500$. The ML constitutive model is defined with a multi-layer perceptron (MLP) with three hidden layers, each containing thirty neurons and using ReLU and SoftPlus as the activation functions. The general architecture of the constitutive model ML is described in detail in Section 3.1.2.

3.1.2 Simulating Load-Controlled Brazilian Disc Experiments

The specimen simulated in Section 1.2.2 is a discretised with a triangular mesh, as shown in Figure 15. The displacement field is approximated with cubic polynomial basis functions. The ground truth constitutive law is a nonlinear function of the strain tensor: the two lamé parameters are defined as:

$$\lambda = 2c_1, \quad \mu = c_1 \frac{1}{1 + c_2 |\text{tr}(\boldsymbol{\varepsilon}(u))|}, \quad (13)$$

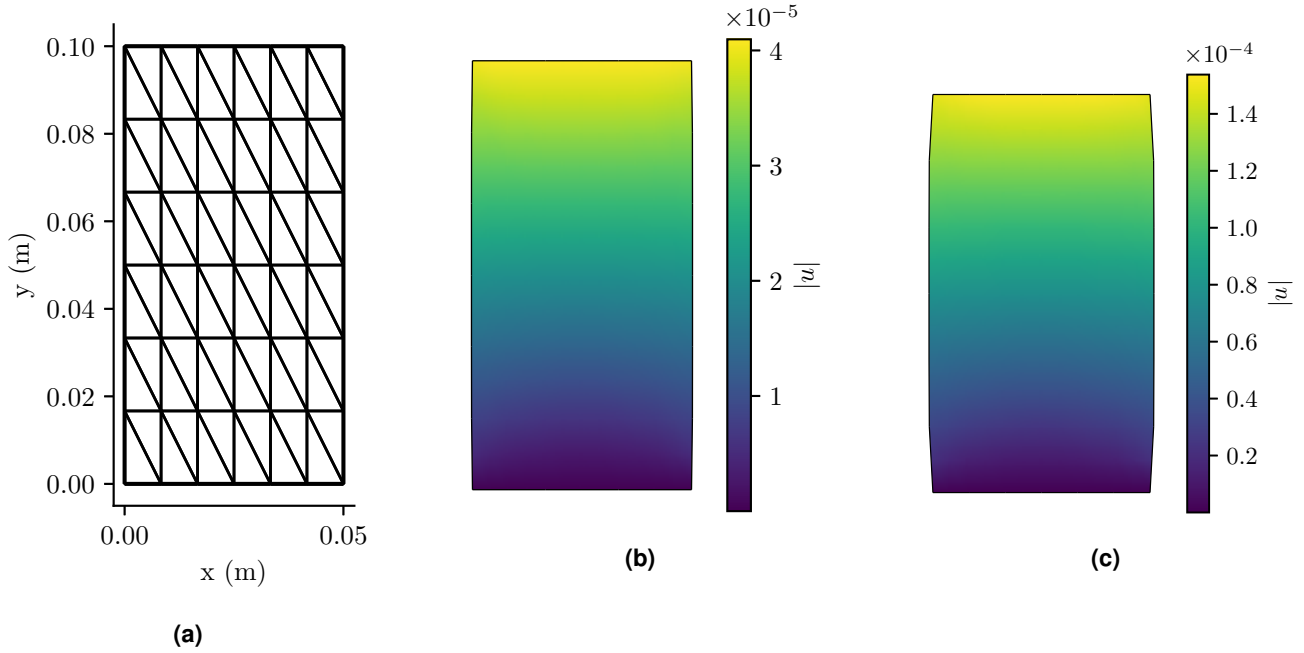


Figure 14. Displacement-Controlled Experiments: (a) computational mesh, displacement magnitude at the (b) first and (c) last loading increment of the training data. The deformation has been amplified by fifty times for visualisation.

where $c_1 = 10^9$ and $c_2 = 500$.

Instead of learning an arbitrary map from strain to stress, we parameterise the constitutive operator through a symmetry-preserving construction. A direct strain→stress network implicitly spans a general fourth-order tangent \mathbb{C} whose coefficients may depend on strain measures and state variables, but offers no guarantees of physical admissibility. Here, the architecture enforces by construction the fundamental requirements of continuum mechanics: frame indifference (objectivity), symmetry of the Cauchy stress, and—when applicable—major symmetry (reciprocity) and material symmetries. Constraining the hypothesis space to symmetry-admissible mappings eliminates non-physical parametrisations, improves data efficiency and identifiability, and provides an analytic consistent tangent via the chain rule, which in turn promotes robust FEM convergence during training.

For isotropic hyperelasticity, these symmetries reduce a generic \mathbb{C} (36 components) to two scalar coefficient functions of the strain invariants. In the small-strain setting we therefore represent the operator with two Lamé-like moduli $\lambda(I_1)$ and $\mu(I_1)$, where $I_1 = \text{tr}(\varepsilon(u))$. Each modulus is learned with a compact MLP that takes I_1 as input, thereby retaining the isotropic tensor basis while permitting non linear dependence on deformation. This choice encodes the required symmetries exactly and yields closed-form algorithmic tangents; it also extends naturally to history- or environment-dependent behaviors by augmenting the MLP inputs with state variables (e.g., confining pressure, stress history, density/void ratio) without altering the tensorial structure, and to anisotropic cases by replacing the isotropic basis with one built from the relevant structural tensors.

The ML constitutive model is defined with two MLPs, one for each of the two lamé parameters, with three hidden layers, each containing thirty neurons and using ReLU and SoftPlus as the activation functions. The input of the two MLPs is the first invariant of the strain tensor, and the output of each MLP is the corresponding lamé parameter. These parameters, together with the strain tensor are then used to compute the stress tensor.

3.1.3 Simulating Torsional Behaviour in Thin Plates

The plate simulated in Section 1.2.3 is discretised with the tetrahedral shown in Figure 16. The displacement field is approximated with cubic polynomial basis functions. The ground truth constitutive law is the same nonlinear function used for the training in Section 1.2.2.

3.2 Transient thermodynamics problem formulation

We consider a transient heat conduction problem on two bodies, where the thermal conductivity of one of the two bodies is a non-linear function of temperature. This problem is governed by the time-dependent heat equation, expressed as:

$$\rho c_p \frac{\partial T}{\partial t} = \nabla \cdot (k \nabla T), \quad (14)$$

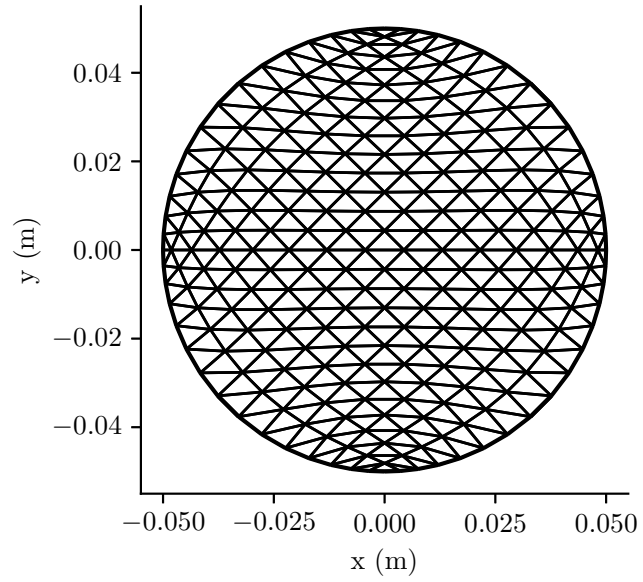


Figure 15. Computational mesh used in the load-controlled Brazilian disc experiment.

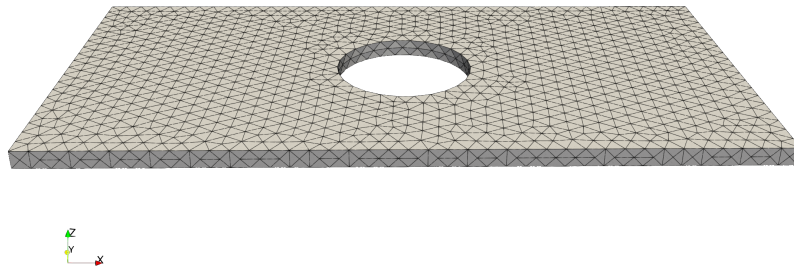


Figure 16. Computational mesh used in the torsion of holed plate experiment.

where T represents the temperature field in Kelvin, ρ denotes the material density measured in kg/m^3 , and c_p is the specific heat capacity, expressed in $J \cdot kg^{-1} \cdot K^{-1}$. The expression $\nabla \cdot (k\nabla T)$ describes the heat flux divergence, while $\frac{\partial T}{\partial t}$ corresponds to the transient variation of temperature. The term k is the thermal conductivity, measured in $W \cdot m^{-1} \cdot K^{-1}$, which can be a non-linear function of temperature and parametrised with a neural network:

$$k = \mathcal{G}_\theta(T). \quad (15)$$

3.2.1 Simulating Transient Heat Conduction Experiments

The two bodies simulated in Section 1.3 are discretised with a tetrahedral mesh shown in Figure 17, where half of the square plate is transparent to show the hole in the circular bottom plate. The temperature field is discretised with linear basis functions. The ground truth thermal conductivity law is a nonlinear function of the temperature defined as:

$$k = k_r \left(1 + \beta \frac{T - T_r}{T_r} \right)^{-\delta} \quad (16)$$

where T is the temperature; $\beta = 1.0$ is a dimensionless constant; $\delta = 0.62$ is an exponent that characterises the temperature dependence; $k_r = 2.0$ is a reference thermal conductivity; and $T_r = 298.0$ K is the reference temperature. The ML constitutive model is defined with an MLP with two hidden layers, each containing thirty neurons and using ReLU and Sigmoid as the activation functions. The input of the MLP is the temperature, and the output is the corresponding thermal conductivity, which is then used to solve the PDE.

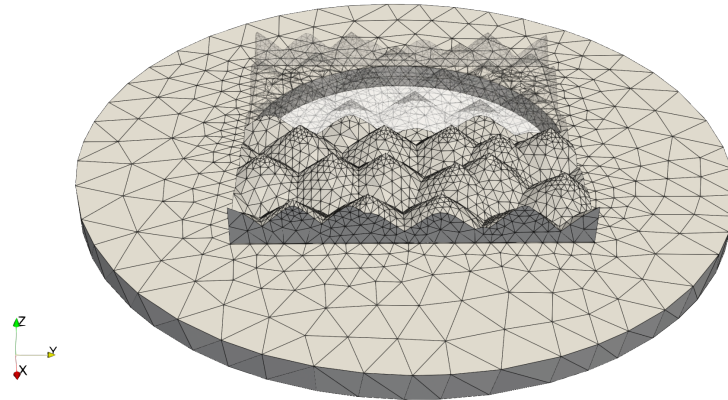


Figure 17. Computational mesh used in the thermal conduction experiment.

Data availability

All data supporting the findings of this study are available within the paper and its Supplementary Information.

Author contributions

A.F.; N.B.: Conceptualization; Methodology; Formal analysis; Software; Validation; Writing - original draft; Writing - review & editing. D.A.H.: Writing - review & editing.

References

1. Karniadakis, G. E. *et al.* Physics-informed machine learning. *Nat. Rev. Phys.* **3**, 422–440 (2021).
2. Bouziani, N., Ham, D. A. & Farsi, A. Differentiable programming across the PDE and Machine Learning barrier. *arXiv preprint arXiv:2409.06085* (2024).
3. Quarteroni, A., Gervasio, P. & Regazzoni, F. Combining physics-based and data-driven models: advancing the frontiers of research with scientific machine learning. *Math. Model. Methods Appl. Sci.* **35**, 905–1071, DOI: [10.1142/S0218202525500125](https://doi.org/10.1142/S0218202525500125) (2025). <https://doi.org/10.1142/S0218202525500125>.

4. Belbute-Peres, F. d. A., Economon, T. D. & Kolter, J. Z. Combining Differentiable PDE Solvers and Graph Neural Networks for Fluid Flow Prediction, DOI: [10.48550/arXiv.2007.04439](https://doi.org/10.48550/arXiv.2007.04439) (2020). ArXiv:2007.04439 [physics, stat].
5. Bouziani, N. & Ham, D. A. Physics-driven machine learning models coupling PyTorch and Firedrake. In *ICLR Workshop on Physics for Machine Learning*, DOI: [10.48550/arXiv.2303.06871](https://doi.org/10.48550/arXiv.2303.06871) (2023).
6. Crilly, A., Duhig, B. & Bouziani, N. Learning closure relations using differentiable programming: An example in radiation transport. *J. Quant. Spectrosc. Radiat. Transf.* 108941 (2024).
7. Li, Z. *et al.* Fourier Neural Operator for Parametric Partial Differential Equations. In *International Conference on Learning Representations* (2021).
8. Li, Z. *et al.* Physics-Informed Neural Operator for Learning Partial Differential Equations, DOI: [10.48550/arXiv.2111.03794](https://doi.org/10.48550/arXiv.2111.03794) (2023). ArXiv:2111.03794 [cs, math].
9. Bartolucci, F. *et al.* Representation Equivalent Neural Operators: a Framework for Alias-free Operator Learning. In *Thirty-seventh Conference on Neural Information Processing Systems* (2023).
10. Bouziani, N. & Boullé, N. Structure-preserving operator learning. *arXiv preprint arXiv:2410.01065* (2024).
11. Ham, D. A. *et al.* *Firedrake User Manual*. Imperial College London and University of Oxford and Baylor University and University of Washington, first edition edn., DOI: [10.25561/104839](https://doi.org/10.25561/104839) (2023).
12. Bouziani, N. & Ham, D. A. Escaping the abstraction: a foreign function interface for the Unified Form Language [UFL]. In *NeurIPS Workshop on Differentiable Programming*, DOI: [10.48550/arXiv.2111.00945](https://doi.org/10.48550/arXiv.2111.00945) (2021).
13. Paszke, A. *et al.* PyTorch: An Imperative Style, High-Performance Deep Learning Library. In *Advances in Neural Information Processing Systems*, vol. 32 (Curran Associates, Inc., 2019).
14. Bradbury, J. *et al.* JAX: composable transformations of Python+NumPy programs. <http://github.com/google/jax> (2018). Version 0.3.13.
15. Ataei, M. & Salehipour, H. XLB: A differentiable massively parallel lattice Boltzmann library in Python. *Comput. Phys. Commun.* **300**, 109187, DOI: [10.1016/j.cpc.2024.109187](https://doi.org/10.1016/j.cpc.2024.109187) (2024). ArXiv:2311.16080 [physics].
16. Holl, P., Koltun, V. & Thuerey, N. Learning to Control PDEs with Differentiable Physics, DOI: [10.48550/arXiv.2001.07457](https://doi.org/10.48550/arXiv.2001.07457) (2020). ArXiv:2001.07457 [physics, stat].
17. Joglekar, A. S. & Thomas, A. G. R. Machine learning of hidden variables in multiscale fluid simulation. *Mach. Learn. Sci. Technol.* **4**, 035049, DOI: [10.1088/2632-2153/acf81a](https://doi.org/10.1088/2632-2153/acf81a) (2023). Publisher: IOP Publishing.
18. Rackauckas, C. *et al.* Universal Differential Equations for Scientific Machine Learning, DOI: [10.48550/arXiv.2001.04385](https://doi.org/10.48550/arXiv.2001.04385) (2021). ArXiv:2001.04385.
19. Brenner, S. C. & Scott, L. R. *The Mathematical Theory of Finite Element Methods*, vol. 15 of *Texts in Applied Mathematics* (Springer New York, New York, NY, 2008), 3 edn.
20. Farsi, A. *et al.* Full deflection profile calculation and young's modulus optimisation for engineered high performance materials. *Sci. Reports* **7**, 46190, DOI: [10.1038/srep46190](https://doi.org/10.1038/srep46190) (2017).